Structural evolution during gelation of pea and whey proteins envisaged by time-resolved ultra-small-angle x-ray scattering (USAXS)

Da Chen[a], Ivan Kuzmenko[b], Jan Ilavsky[b], Lorena Pinho[a, c], Osvaldo Campanella[a,*]

[a] Department of Food Science and Technology, The Ohio State University, 2015 Fyffe Rd, Columbus, OH43210, United States

[b] X-ray Science Division, Argonne National Laboratory, Lemont, Illinois 60439, Unites States

[c] Departamento de Engenharia de Alimentos Universidade de São Paulo, Faculdade de Zootecnia e Engenharia de Alimentos, Pirassununga, São Paulo, Brazil

*Author for Correspondence

Osvaldo Campanella: campanella.20@osu.edu

Abstract

Hydrogels from plant proteins commonly exhibit inferior gel strength compared to those from dairy proteins partially due to their distinct gel networks. How protein aggregates to form such networks in response to heat remains largely unknown. In here, pea (PPI) and whey (WPI) protein isolate gels were produced at the same protein content and similar heating/cooling rate. The process was monitored using rheology, microscopy and *in situ* ultra-small-angle x-ray scattering (USAXS). Rheology showed an initial decrease in G' and G'' in PPI followed by a steady increase when the temperature surpassed ~60°C at 2°C/min heating rate, whereas a much higher temperature (~80°C) was required for WPI. Microscopy showed a coarse and heterogenous network in PPI, whereas for WPI, the network was finer and more continuous. In both gels, nano-sized spherical or ellipsoidal particles were present as the basic constituents. USAXS found individual protein was dominant in PPI or WPI solution at temperature below 57°C. Their proportions decreased together with appearance of aggregates with an average R_g of 9-10 nm in PPI and 6-7 nm in WPI at higher temperature. The size of the aggregates changed slightly during further heating and cooling, but their proportions increased. Power law exponents revealed the aggregates were mass fractals for WPI and PPI gels, and they became more compact during heating. Our findings suggested formation of primary aggregates in protein gel networks is a more organized process than commonly thought and provided theoretical guidance for production of high protein food gels with desirable texture.

Keywords: Plant protein, Dairy proteins, microstructure, rheology, hydrogels, scattering

Highlights

- PPI displayed a coarser and more heterogeneous gel network than WPI at pH7
- PPI and WPI gel were composed mainly of aggregates of a few protein molecules
- Size of the aggregates were not changed but their amount increased during cooling
- The aggregates were surface fractals for both gels and larger in size in PPI gel

Graphic Abstract

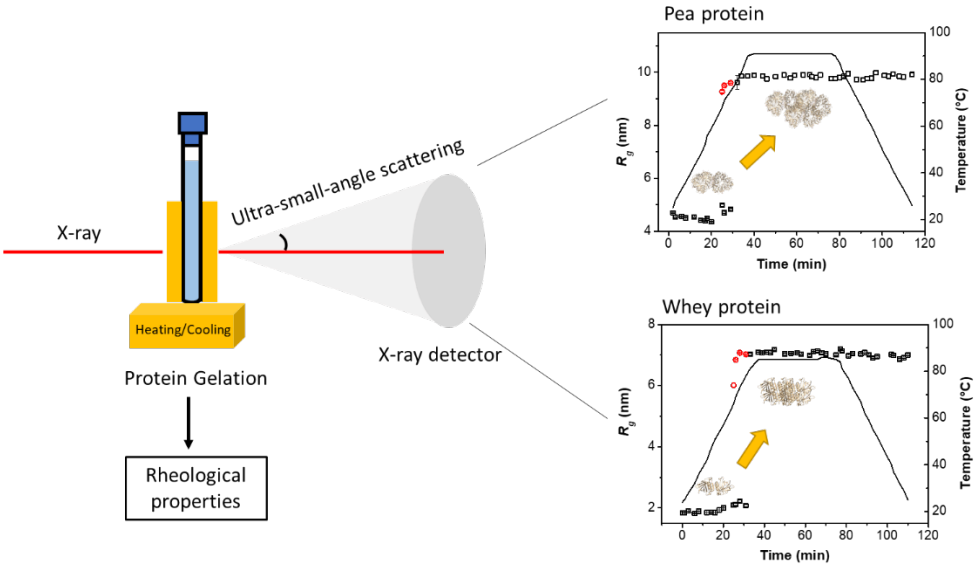

1. Introduction

Protein-based food gels are the main structural skeletons and textural providers of varies types of foods. In them, proteins require to interact with themselves or non-protein components to form a three-dimensional network (Nicolai, 2019; Chen et al. 2020). Depending on the source of proteins and the production conditions, the structure of the final gels differs significantly, so as their gel viscoelasticity (Chen et al. 2021; McCann, Guyon, Fischer, & Day, 2018; Mahmoudi, Mehalebi, Nicolai, Durand, & Riaublanc, 2007).

Heating is the most common approach to induce protein gelation. During the process, proteins unfold and aggregate until a self-supporting network is built (Chen et al. 2021). The dimension/morphology of the aggregates has been demonstrated to largely determine the microstructure of the gel (Weijers, Visschers, & Nicolai, 2002). Whey proteins, by-products from cheese production, contain mainly β-lactoglobulins (~60%) and α-lactalbumin (20%), with a small proportion of BSA and immunoglobulin G. (Ramos et al. 2012). They are well known to form a homogenous fine-stranded network composed of mainly nano-sized aggregates at low ionic strength and neutral pH by heating (Ako, Durand & Nicolai, 2011; Wagner, Biliaderis, & Moschakis, 2020), with a storage modulus of a few hundred to several thousand Pa depending on the protein concentration used (Fernandes, 1994). Under similar conditions, pea proteins, a mixture of globulin (legumin, vicilin and covicilin, 50-60%) (Boye, Zare, & Pletch, 2010) and albumin (15-20%) (Yang, Zamani, Liang, & Chen, 2021), their gel networks are more heterogeneous, consisting of strands, beads and large aggregates with dimensions ranging from smaller than 30 nm to over a few hundred nm (Munialo, van der linden & de Jongh, 2014; Chen et al., 2021), and possessed much weaker gel strength (Yang et al. 2021; Chen et al. 2021). The difference originates from protein unfolding, aggregation, agglomeration of aggregates to form networks as well as network restructuring (Nicolai, 2019). Tacking those key steps is of vital importance to understand the mechanisms of gel formation

of plant and dairy proteins under heat so as to unravel their difference on gel strength from the structural aspect, even though chemical forces also contribute (Brodkorb, Croguennec, Bouhallab, Kehoe, 2016; Chen et al. 2021).

Confocal and electron microscopy have been widely employed to examine the microstructure of protein gels. The former enables to maintain the gels at hydrated status and even track their formation with a resolution of a few hundred nm to μm (Ko & Gunasekaran, 2009). The technique is ideal for gels composed of microparticles, but not for those with fine-stranded networks (Nicolai, 2019). Electron microscopy possess nano-meter resolution, but sophisticated sample pre-treatments could bring artefacts. In addition, it applies mainly to the gels rather than protein solutions/suspensions or the intermediate status. Ultra-small-angle x-ray scattering (USAXS) is a non-destructive measurement technique capable of acquiring the information about the size, shape, volume and total surface area of the scatters with appropriate mathematical modelling (Ilavsky et al. 2009). It has been applied to protein solutions (Da Vela et al. 2016), dispersions (Banc et al. 2019) and gels (Chen et al. 2021; Tsung, Ilavsky & Padua, 2020) for characterization of their structural units at multiple length scales (from nm to μm). Combined with synchrotron radiation, monitor the changes of scatters in response to external environments such as heat can also be achieved (Banc et al. 2019). Due to these advantages, *in situ* characterization of heat-induced gelation of food proteins by USAXS would provide insightful information regarding protein aggregation that can not be envisaged by other techniques.

In the present study, pea and whey protein solutions were prepared at the same protein content. Their scattering patterns were recorded on USAXS instrument during the gelation process under heat/cooling. Mathematical models (Ilavsky & Jemian, 2009; Ilavsky et al. 2009) were then used to obtain the size, shape and size distribution of proteins or their aggregates during gelation which were later compared with microscopy. The gelation dynamics of the two

protein solutions under similar conditions were also monitored using rheology aiming to reveal the structure-texture correlation.

2. Materials and Methods

2.1 Materials

Whey protein isolate (WPI) was acquired from Hilmar™ Ingredients (Hilmar, CA, USA) with a reported 89.7% (w/w) protein content, 2.6% ash, 0.6% fat and 0.2% lactose. Dry split pea was purchased from local supermarket. Analytical grade NaOH, monopotassium and dipotassium phosphate was obtained from Thermo Scientific. Glutaraldehyde (25%, w/v) was obtained from Sigma Aldrich. NMR tube (4.2-mm ID) was purchased from Norell Inc. (Morganton, NC, USA). Water used was de-ionized.

2.2 Isolation of pea proteins

Dry split pea was ground to make pea flour. The flour was defatted with hexane as described previously (Stone, Karalash, Tyler, Warkentin, & Nickerson, 2015). The defatted flour was mixed with water in a ratio of 1:10 (w/v), adjusted to pH9.5, stirred for 1 h and centrifuged (16640× g, 20 min, 4°C). The supernatant was collected, adjusted to pH4.5 and centrifuged (13750× g, 10 min, 4°C). The sediment was collected, mixed with water, adjusted to pH6.5 and freeze-dried (Chen et al. 2021). The protein content in the freeze-dried samples (PPI) was measured to be 86% by a nitrogen analyser with a conversion factor of 6.25. It contained mainly vicilin, convicilin and legumin from SDS-PAGE (**Fig. S1**).

2.3 Rheology

PPI and WPI was added to de-ionized water and stirred for 5 h to make a solution containing 13% (w/w) proteins. Such a protein concentration was used to guarantee the formed gels possessed moderate to high viscoelasticity. Their pH was then adjusted to 7 using 2 N NaOH and stirred for 1 h. The solutions (~25 mL) were loaded to the DHR-3 rheometer (TA

instrument, New Castle, USA) equipped with a standard Peltier Concentric Cylinder geometry including a cup (30 mm diameter) and a Recessed End Rotor (28 mm diameter and 42 mm height). A solvent trap cover was placed on top of the cup to minimize water loss. The temperature of the PPI solution was ramped from 25 to 90°C at a rate of 2°C/min, kept at 90°C for 30 min and cooled down to 25°C at a rate of 2°C/min. For WPI, it was heated from 25 to 85°C, kept at 85°C for 30 min, and cooled down to 25°C, with a 2°C/min heating and cooling rate. Higher maximum temperature was used for PPI because they were more resistant to heat compared to those of WPI (Kornet et al. 2021; Fitzsimons, Mulvihill, & Morris, 2007). The storage modulus (G') and loss modulus (G'') were recorded during gelation at 1Hz frequency and 1% strain (linear viscoelastic region). Duplicates or triplicates were run for each sample.

2.4 Microstructure

PPI or WPI solution (13%, w/w) was mixed with 0.2% (w/v) rhodamine B in a proportion of 50:1 (v/v) for 30 min at room temperature in dark. Unbound dyes were removed by dialysis (10 K MWCO) against water for 48 h. The retentate was freeze-dried and solubilized in water to reach a protein content of 13% (w/w). An aliquot (~40 µL) was transferred to a concave slide, sealed using epoxy glue and heated to form gels on the Peltier plate installed on the DHR-3 rheometer using the same condition as described above. Samples were taken at different temperatures during gelation and imaged using Zeiss LSM900 Confocal Laser Scanning Microscope (CLSM) (Oberkochen, German) with a 63× oil lense (Chen et al. 2021).

For SEM, PPI or WPI gel was prepared in a 200 µL pipette tips in the concentric cylinder on DHR-3 rheometer under the same condition as described above. The tips were cut to short segments, fixed using 2.5% glutaraldehyde for 16 h, dehydrated with different concentrations of ethanol, critical point dried, sputtered coated with gold palladium and imaged using Quattro ESEM (Chen et al. 2021) at an accelerating voltage of 5 kV and a pressure of 20-30 Pa.

205 *2.4 Ultra-small-angle x-ray scattering (USAXS)*

206 PPI or WPI solutions (13%, w/w) in NMR tubes were vacuumed for 20 min and incubated in
207 ice bath for 30 min to remove air bubbles. They were then loaded into a custom-designed
208 heating/cooling system installed on the USAXS instrument at 9-ID-C beamline at the
209 Advanced Photo Source, Argonne National Laboratory. Gelation of the protein solutions were
210 conducted with a programmed heating and cooling temperature profile matching the one used
211 for the rheology measurements. The actual heating rate and cooling rate was measured to be
212 ~1.7-2°C/min. Absolutely calibrated USAXS data was collected every 2-5 mins during gelation
213 with an X-ray energy of 21 keV, a 5×10^{12} $mm^{-2}s^{-1}$ photo flux and a 90 s measurement time
214 (Ilavsky et al. 2013, 2018). The obtained range of scattering vector Q was between 1×10^{-4} $Å^{-1}$
215 and 0.3 $Å^{-1}$. $Q = 4\pi\frac{\sin(\theta/2)}{\lambda}$, where λ is the x-ray wavelength, and θ is the scattering angle.
216 Scattering intensity of solvent background and the sample holder was subtracted before data
217 analysis.

218 A multi-level unified fit (Beaucage, 1995) was used to fit the scattering data generated by the
219 Irena package (Ilavsky & Jemian, 2009). This model assumes protein systems (including
220 suspensions, gels and the intermediates) had sizes of different dimensions (structural levels),
221 such as native proteins, building blocks and/or the large fractal structure. Each level would
222 generate a Guinier regime which corresponds to the characteristic sizes (radius of gyration, R_g),
223 and a power law slope (P) reflecting the shapes of the scatters with assumption that the
224 interactions among scatters have limited effects on the scattering signals (**Fig. S2**). The model
225 also assumes limited or no interactions among scatters. The radius of gyration (R_g) and the
226 structurally limited power law (P) of aggregates of various size were acquired from the fitting
227 method according to the following equation:

$$I(Q) = \sum_{i=1}^{n} G_{\mathrm{i}} \exp\left(\frac{-q^2 R_{\mathrm{gi}}^2}{3}\right) + B_{\mathrm{i}} \exp\left(\frac{-q^2 R_{\mathrm{g(i-1)}}^2}{3}\right) \left[\frac{(\mathrm{erf}\left(\frac{qR_{\mathrm{gi}}}{\sqrt{6}}\right))^3}{q}\right]^{P_i} + I_{bkg} \qquad (1)$$

Where i represents structural level, R_g is the intensity weighted average radius of gyration of scatters, P_i is the power law exponent, G_i is the Guinier scale and B_i is the perfector of power-law scattering at structural level i.

A modelling tool was used to analyse the size distribution of the scatters during gelation using Irena package with a limited number of bins in radii according to the following equation that considers the interference between scatters (Ilavsky & Jemian, 2009).

$$I\ (\mathrm{Q}) = \sum_k |\Delta\rho|^2\, S_k(Q) \sum_{j_k} |F_k(Q, r_{jk})|^2\, V_k(r_{jk}) f_k(r_{j_k}) \Delta r_{j_k} \qquad (2)$$

where subscript j includes all bins in the size distribution and Δr_j is the width of bin j. Subscript k denotes different populations with each has a binding index j_k. r is the radius of the scatter. $|\Delta\rho|^2$ is the scattering contrast, $S\,(Q)$ is the structure factor. $F(Q, r)$ is the scattering form factor, $V(r)$ is the volume of the scattering particle. $f\,(r)$ is the volume size distribution calculated as:

$$f(r) = V(r) * N(r) = V(r) * N_T\, \psi(r) \qquad (3)$$

$V(r)$ is the volume of the scatter, $N(r)$ is the number distribution, N_T is the total number of the scatter, and $\Psi(r)$ is the probability of occurrence of scatter at size of r. $f\,(r)$ was assumed to follow as log-normal distribution.

Native and unfold proteins, as well as protein aggregates are non-spherical particles according to literature (Kaieda, Lund, Plivelic, & Halle, 2014; Ikeda & Morris, 2002; Chen et al. 2021). The aggregates may present as fractals in gels but considering their compact structures (with no appearance of Guinier regime for its constituents), we assumed they were spheroids with an aspect ratio smaller than 0.99 as native and unfold proteins. This reduced uncertainty of fitting

because fractal model involves in multiple variables whose values change significantly with the initial guesses. $F(Q, r)$ can be thus calculated as shown below:

$$F(Q,\mathrm{r}) = \int \left(\frac{3}{(Q_r)^3}\right) (\sin(Q_r) - (Q_r \cos(Q_r)))dr \quad (4)$$

where $Q_r = Q \times r \times \sqrt{1 + (ar^2 - 1)) \times (\cos\theta)^2}$, $0 \leq \cos\theta \leq 1$.

The structure factor ($S(Q)$) used in the present work accounts for weak correlation between colloidal particles including the extent of correlation and spatial distance. Correlation commonly occurs among protein molecules at high concentration. The *S(Q)* can be calculated as (Beaucage, Ulibarri, Black, & Schaefer, 1995):

$$S(Q) = \frac{1}{1+k\frac{3(\sin(Q\zeta)-Q\zeta(\cos(Q\zeta)))}{Q\zeta^3}} \quad (5)$$

where k describes the degree of correlation with a value between 0 to 6, ζ is the interaction distance of spheroids, which is no less than R_g.

3. Results and Discussion

3.1 Gelation dynamics

Rheological properties of protein solutions or gels associate closely with their molecular rigidity and interactions which can be manipulated by thermal stress. Monitor the G' and G'' during gelation of the proteins by time sweep is a commonly adopted strategy to indirectly reflect their structural and interaction changes in the system. **Fig. 1** showed an initial decrease of G' and G'' of PPI, which is probably due to decreased viscosity of the system (water, protein molecules) as well as dissociation of protein clusters (Comfort & Howell, 2002). In addition, under moderate heat, non-covalent interactions between protein molecules might be weakened because of increased molecular distance from accelerated Brownian motion (Woldeyes, Wei, Razinkow, Furst, & Roberts, 2020). The moduli increased rapidly when the temperature

surpassed ~60°C, suggesting proteins start to unfold and aggregate to form networks. The physicochemical events continued at further heating, as evidenced from increased moduli. More evident increments of G' and G'' were observed at the cooling stage, indicating formation of more cross-links/interactions or re-structuring of networks which could increase the resistance of the bonds between proteins to stretching and/or bending (Sun & Arntfield, 2011; Nicolai, 2019). For WPI, it showed a similar trend as those in PPI except the rapid increase of moduli occurred at higher temperature (~80°C) with a faster rate. *β*-lactoglobulin, the major component of whey protein isolate, has been reported to have a similar behaviour during gelation (Huang, Catignani, Foegeding & Swaisgood, 1994). It must be noted 277 that the measured gel temperature depends on the temperature ramp, therefore it cannot be 278 defined as a true critical temperature. At a lower heating rate, protein molecules have more 279 time to unfold and re-arrange, resulting in cross-link at lower temperatures. Conversely, the 280 time for such events is not sufficient at higher heating rate, thus proteins are gelled later (Sun 281 & Arntfield, 2011). The increment of G' in the cooling stage of WPI had a smaller contribution to the final G' of the gel in relative to PPI. This implies that most of the colloidal aggregation in WPI gel were completed prior to cooling. WPI gel had much higher G' and G'' than those of PPI even though the same concentration was used. Formation of networks with distinct microstructure could be one reason (Koret, Shek, Venema, vander Goot, Meinders, & van der Linden, 2021). The other reason is the significant role of covalent interactions (disulphide bonds) in stabilization of the gel network (Wagner, Biliaderis, & Moschakis, 2020), which is nearly negligible in PPI gels (Sun & Arntfield, 2012; Chen et al. 2021).

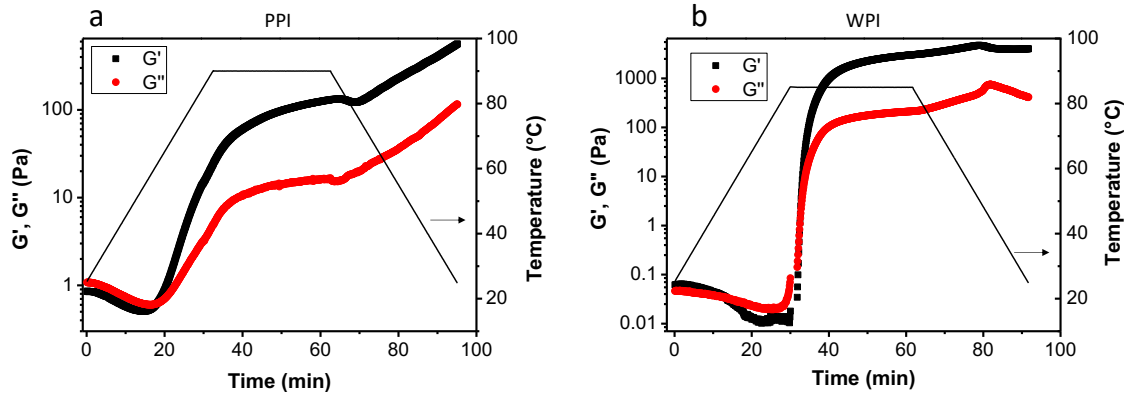

Fig 1. Temperature sweep of 13% (w/w) pea protein isolate (PPI) (**a**) and whey protein isolate (WPI) (**b**) in distilled water at pH7.

3.2 Micro- and nanostructure during gelation

Protein gel networks vary significantly with pH and ionic strength. They are mainly presented as connected aggregates (Wagner et al. 2020). These aggregates differ in size, shape and arrangements, depending mainly on the source of proteins and the heating conditions. Microscopy and x-ray scattering experiments were thus conducted to acquire such information to explain the difference on the gelation dynamics between PPI and WPI. CLSM images (**Fig.2a-j**) showed that PPI and WPI proteins were well dispersed in the solutions. The former showed relatively larger size, indicating presence of aggregates. Similar findings have been reported in our previous study (Chen et al. 2021). This could be either due to the formation of protein clusters in concentrated system (Porcar et al. 2010) or denaturation of some proteins during protein isolation. Once gelled, PPI displayed sparely distributed clusters/aggregates of various sizes, whereas they were more homogenous without recognizable dimension in WPI, indicating much denser networks. Consistent with CLSM results, SEM showed larger voids or even cracks in PPI gel network compared to WPI. In addition, the protein aggregates in PPI gels were heterogenous, showing as irregular shape and varied size ranging from less than 30 nm to more than 200 nm (**Fig. 2k, l**). And small aggregates were dominant in the gel network (**Fig. 2k**). For those with large size (> 200 nm), multiple small spherical or ellipsoidal particles were seen as the constituents. It has been reported previously that pea protein gels formed

network dimensions smaller than 50 nm (Munialo, Linden & de Jongh, 2014), which agrees well with the present findings. In the WPI gels, ellipsoidal particles of 20-50 nm were dominant and presented as bead string to form interconnected network (**Fig. 2m, n**). At neutral pH, ellipsoidal particles with a thickness of 11-27 nm were reported in heat denatured WPI solution at low concentration (Ikeda & Morris, 2002) by atomic force microscopy. Somewhat larger on size obtained in the present study might be caused by the coating materials.

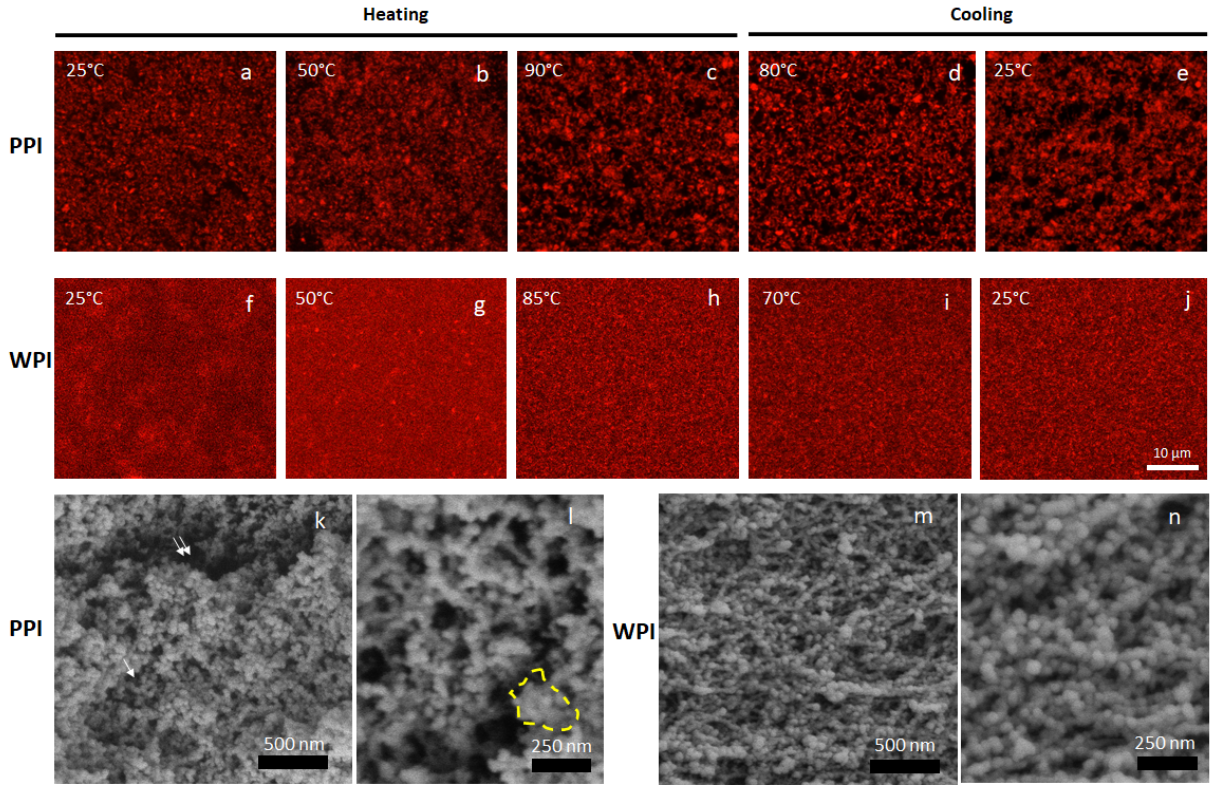

Fig. 2. Confocal (**a-j**) and scanning electron micrographs (**k-n**) of PPI (**a-e**, **k-l**) and WPI (**f-j**, **m-n**) solutions or gels. Appearance of PPI **(a-e)** or WPI (**f-j**) system at different temperatures during heating and cooling process. Proteins were stained with Rhodamine B before heating. (**k-l**) Network structure of PPI gel. Double and single arrow(s) in **k** highlights the location of cracks and voids. The irregular shape with dashed line in **l** denotes the large aggregates. (**m-n**) Network structure of WPI gel. PPI, pea protein isolate; WPI, whey protein isolate

Even though SEM directly showed the gel microstructure, it may induce artifacts due to dehydration, critical point drying and coating required by this technique. Also, it fails to track

the aggregation process during gelation. Synchrotron USAXS was thus employed to overcome the shortcomings and provide extra information regarding changes of size and shape of protein molecules or aggregates induced by heating. Scattering patterns of PPI solution showed a Guinier regime centred at ~0.05 $Å^{-1}$. At lower Q region (<0.01 $Å^{-1}$), the scattering curves were upturned instead of horizontal, indicating the presence of protein clusters or aggregates with larger dimensions. At high concentration, the mobility of proteins is reduced due to excluded volume effects. In this crowed media, protein-protein distance decreases resulting in the formation of self-associated clusters via mainly non-covalent interactions (Saluja & Kalonia, 2008; Doster & Longeville, 2007). The possibility that a small proportion of proteins were aggregated during protein isolation should not be entirely ruled out. The Guinier regime in the solution gradually disappeared with appearance of a new shoulder at ~0.01 $Å^{-1}$ during heating (**Fig. 3a**). Meanwhile, the intensity of the region at Q < 0.009 $Å^{-1}$ increased. These clearly indicate aggregation of proteins to form larger structures. Similar phenomenon was observed in WPI (**Fig. 3b**). However, in either its solution or gel, the Guinier regimes were more evident and located at higher Q compared to the PPI counterparts, suggesting presence of smaller structural units with less polydispersity (Chen et al. 2021). When reaching to the lower Q, a flat plateau was shown in the samples below 73 °C. The flat plateau disappeared at higher temperatures or during cooling stage indicating increased protein interactions and polydispersity of the system (McEwan, Egorov, llavsky, Green & Yang, 2011; Vogtt, Javid, Alvarez, Sefcik & Bellissent-Funel, 2011). In both PPI and WPI, a clear iso-scattering point was observed regardless of heating temperature, similar observation has been found in β-LG and ovalbumin (Nicolai, Pouzot, Durand, Weijers, & Visschers, 2006). This is due to reduction of the fraction of native proteins and concomitant formation of aggregates with the same local structure.

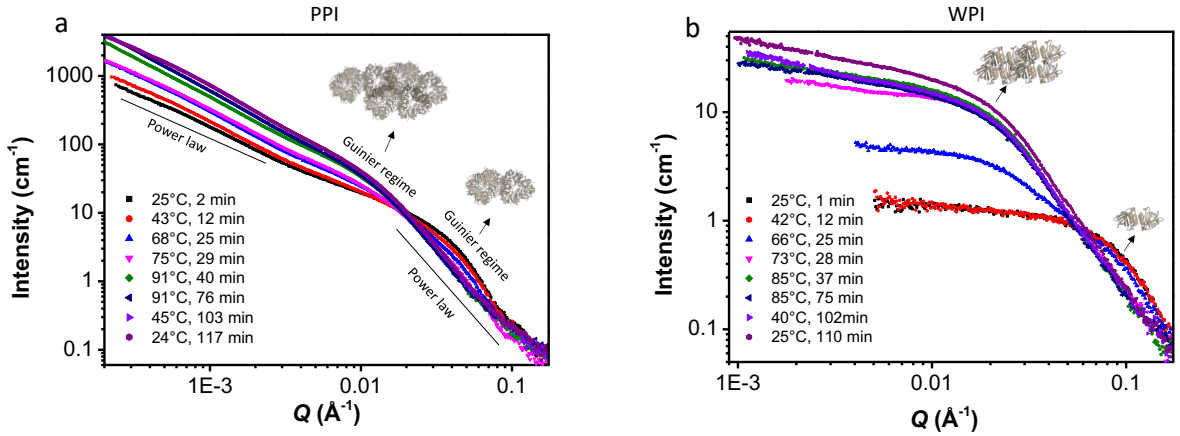

353

354 **Fig. 3**. Ultra-small-angle x-ray scattering patterns during *in-situ* gelation of PPI (**a**) and WPI
355 (**b**) solutions. PPI and WPI had the same protein concentration (13%, w/w). The protein
356 solutions were heated to reach maximum temperature (~1.7 °C/min), maintained for half an
357 hour, then cooled down to room temperature (~2 °C/min). The Guinier regime and the
358 following power law slope of the scattering pattern were labelled on **a**. Guinier regimes which
359 represent scatters of different size were also highlighted with protein trajectories. The power
360 law slope reflects the shape of the scatters.

361

362 Using unified fit (**Fig. S3**), an R_g (*Radius of gyration*) value of ~4.5 nm for PPI before
363 heating (**Fig. 4a**) was obtained, corresponding to individual protein molecule of 7S and 11S
364 globulins (Miles et al. 1985), which were unable to be examined by using CLSM or SEM due
365 to their limited resolution. The R_g value decreased initially during heating (from 0 to 20 min)
366 even though slight fluctuation occurred. Similar observation has been found previously when
367 heating β-conglycinin and glycinin under acidic or alkaline condition (Xiao et al. 2016). This
368 might be attributed to the change of protein shape or release of some polypeptides from
369 hexamers. The power law exponent (P) of the proteins (with a R_g value of 4-5 nm) decreased
370 from 2.76 at 25 °C to 2.20 at 59°C (**Fig. 4c**), suggesting they become less compact and more
371 plane-like structures (Chen et al. 2021). Continued heating promoted PPI unfolding and
372 aggregation, resulting in the presence of two dominant structures of distinct sizes in the system.
373 One had a R_g value of ~5 nm with a P value of 1-2, indicating the protein molecule were
374 unfolded with a thread-like feature. The other was 9-10 nm possessing a P value of 2-3 (**Fig.**

375 **4a**). The structure represents aggregates of a few protein molecules in a form of mass fractals.
376 In our previous study (Chen et al. 2021), aggregates with larger R_g value (~16 nm) were
377 dominant in PPI gel. The discrepancy could arise from distinct heating conditions and protein
378 content used. Between 65-80°C, the R_g and P value increased with the temperature, indicating
379 occurrence of extensive protein aggregation and the aggregates became more compact. Once
380 reached to the maximum temperature (91°C), the R_g and P values of the aggregates changed
381 slightly upon further heating and cooling. At these stages, most of the proteins are involved in
382 aggregation to form gel network as shown in rheology and microstructure, which favours local
383 re-structuring. Alternatively, the surface charge of proteins could increase with aggregation
384 and provide strong repulsion force which limits further aggregation (Nicolai, 2019).

385 In the WPI solution, the R_g value was ~1.8 nm at 25 °C (**Fig. 4b**). Dimers of β-lactoglobulin
386 has been reported to have similar size (Vogtt et al. 2011). Further changes of R_g followed path
387 similar to those of PPI during heating, including the presence of two populations with distinct
388 sizes at the end of heating stage and slightly varied R_g values in the plateau and the cooling
389 stage. R_g value of the aggregates in WPI gel was ~4 times as that of the single protein compared
390 to ~2.5 in PPI, suggesting higher number of protein molecules were included in the aggregates
391 and those aggregates are compact with little internal structure. Two-step aggregation
392 mechanism of whey proteins or β-lactoglobulin has been proposed previously during heating
393 (Ikeda & Morris, 2002; Aymard, Gimel, Nicolai, & Durand, 1996; Vijayalakshmi, Krishna,
394 Sankaranarayanan, & Vijayan, 2008). The first step consisted in formation of small particles
395 (radius 6-8 nm), and in the second step, the particles are organized to form fractal structures.
396 This may apply to the current case and the small particles were the dominant scatters in the gel.
397 The P value decreased from 3.3 to ~2 during heating, suggesting conversion of whey proteins
398 from surface to mass fractals characterized by a loosed conformation. Further heating and
399 cooling increased P values to ~2.8, indicating the primary protein aggregates were more

compact and denser compared to those of denatured whey proteins, which is probably due to rearrangements driven by covalent and non-covalent interactions. The large aggregates may further organize to even larger structure that beyond the measurement limit of USAXS (more than a few μm). Those larger structures had a rod-like shape as demonstrated from the *P* value close to 1.

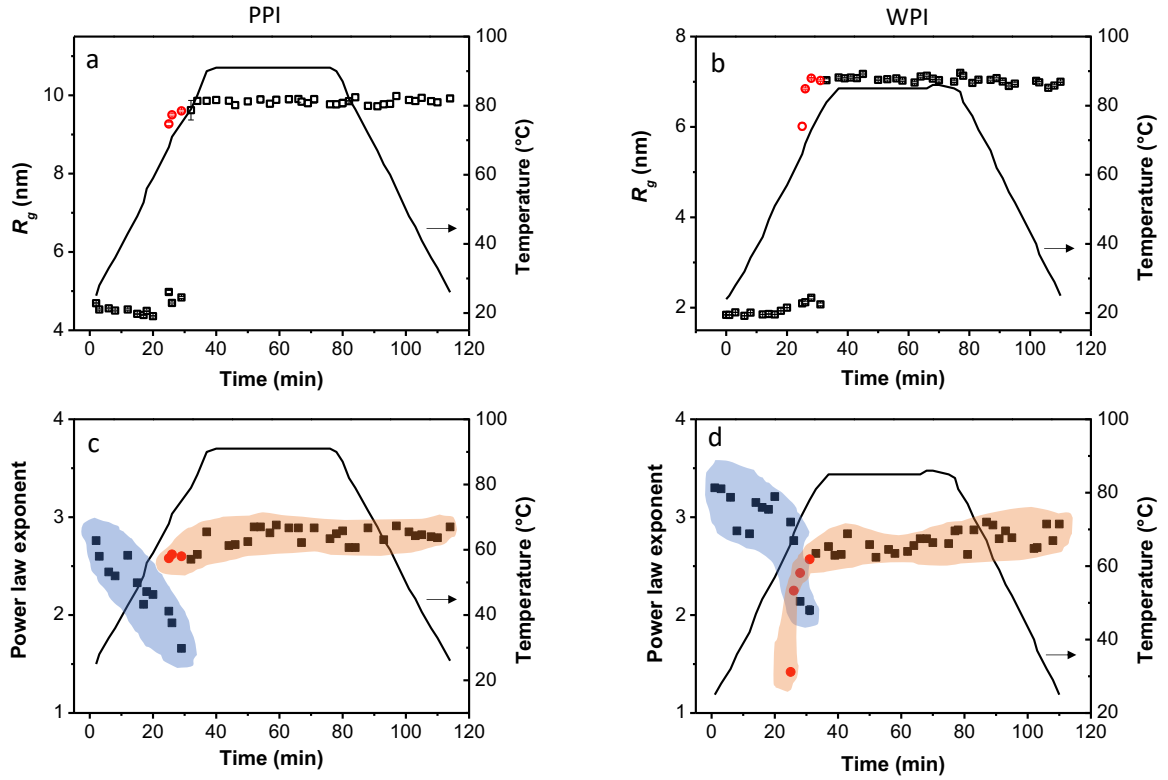

Fig. 4 Change of radius of gyration (**a**, **b**) and power law exponents (**c**, **d**) of dominant scatters during gelation of PPI (**a**, **c**) and WPI (**b**, **d**) derived from the unified fit along the temperature profile applied to the cooling heating process. The red round symbols denote appearance of protein aggregates when individual protein existed. The irregular shapes filled with light blue or light pink denote the power law exponents of individual protein and its aggregates, respectively. The solid lines represent the temperature profiles during gelation.

The R_g value from the Unified fit is the volume weighted average over dimensions of the dominant structures. To further analysis of their size distribution, modelling of the scattering pattern with consideration of the form factor as well as the interference of the scatters was conducted (**Fig. S4**). The median radius of PPI and WPI at different stages of gelation was

similar to the R_g value (**Fig.5**). The size of PPI distributed mainly from 5-10 nm in solution, whereas 2-4 nm in WPI. This indicates both single protein and small aggregates were present. Heating shifted the size to larger values with more broaden distribution. For example, the radius distributed mainly from 5-30 nm in PPI at 91°C (41 min) and 4-16 nm in WPI at 85°C (37 min). Assuming the aggregates are ellipsoids in both gels, the size can be at least 10-60 nm and 8-32 nm in one dimension, which agrees well with the SEM measurement after subtraction the thickness of the coating layer (5-10 nm) (Steyer, Schertel, Nardis & Möbius, 2019). The narrower range of the size distribution in WPI gel denotes constituents were more homogenous than those of PPI. This again was confirmed by CLSM and SEM. From the size distribution, we also found the volume of the aggregates increased during the cooling stage, even though they showed similar median values. Such an information can be hardly acquired from microscopy as defining the boundary of aggregates were implausible. O'Kane et al. (2004) have reported that during the cooling process, agglomeration of the aggregates into a network structure by interaction of exposed residues continued. The size distribution acquired from fitted models did not include the very low-Q (Q< 0.005 Å^{-1}) region which represent larger structures. Since no Guinier regime was present in this region, their proportions in the gels should be limited.

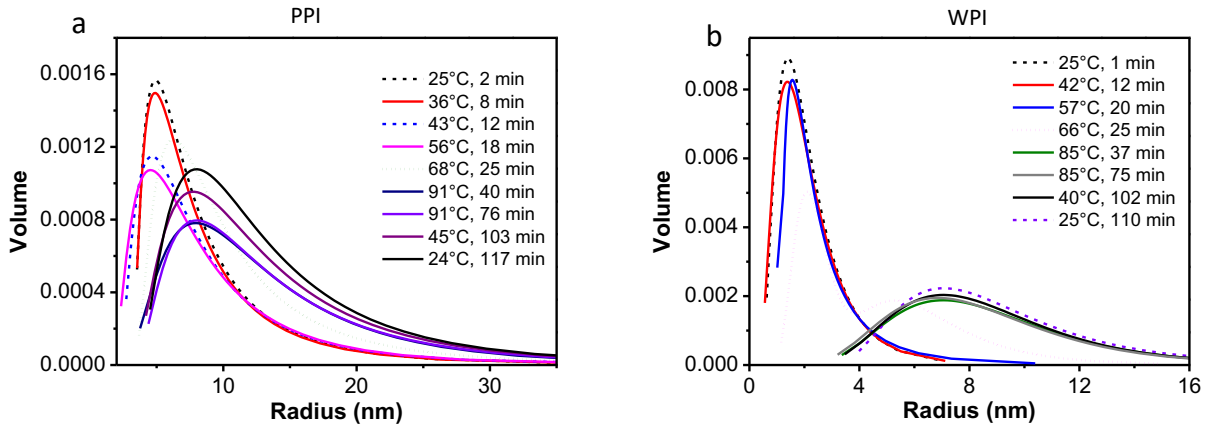

435 **Fig. 5**. Log-normal size distribution of scatters in PPI (**a**) and WPI (**b**) during gelation derived
436 from modelling fitting. Peaks of distribution curve represents the median size of the scatters
437 (individual proteins and/or their aggregates)
438
439 *3.3 Microstructure- rheology relationships during gelation*

440 According to USAXS, the gelation process of PPI and WPI were similar, which include protein
441 denaturation, aggregation and further connection to form networks. Protein aggregation
442 occurred at similar temperatures for PPI and WPI, and once the aggregates were formed, their
443 average size was changed slightly during further gelation. More importantly, the aggregates
444 directly affected the overall appearance of gel networks. It is still under debate whether the
445 strength of protein gels correlates with their microstructure. A lack of univocal correlation was
446 reported on both plant (Urbonaite, De Jongh, van Der Linden, & Pouvreau, 2015; Chen, Zhao,
447 Chassenieux, & Nicolai, 2017) and whey proteins (Mehalebi, Nicolai & Durand, 2008) as
448 protein-protein interactions also contribute to the gel stiffness, whereas some others found
449 protein gel networks with large aggregates, and high discontinuity and coarseness commonly
450 showed lower moduli (Munialo, van der Linden, & de Jongh, 2014) or fractural strain (Picone,
451 Takeuchi, & Cunha, 2011). Our findings cannot exclude the role of homogenous and finer
452 networks in WPI in contributing to its higher G' and G'' in the gel compared to PPI. And for
453 the finer networks, the interacting surface of proteins were larger, resulting in formation of
454 more cross-links. It has to be noted that the microstructure-rheology correlation mentioned
455 above were specific for the gels, not for systems prior to that. During the denaturation stage,
456 both whey and pea proteins were in a solution, their rheological properties decreased slightly
457 with increasing temperatures within a moderated range, which is a typical phenomenon for
458 most solutions. A time lag between the formation of aggregates and the increased moduli
459 suggests the amount of aggregates have to reach a certain threshold before a distinct increment
460 on the moduli.

The microstructure-rheology correlation found PPI and WPI was based on the condition at pH7 with low salt, a widely used environment for production of protein-based gels. Altering the gel formation conditions, such as pH, salt and protein concentration may induce distinct aggregation behaviour of proteins and gel viscoelasticity, which requires further study. Also, in real food gel system, proteins commonly exist with other food components such as polysaccharides, lipid and phytochemicals (Banerjee & Bhattacharya, 2012). The interactions among different food polymers are most likely to affect the thermal response of the proteins during gelation. Since USAXS is not able to distinguish scattering signals in the mixture from their chemical nature, acquiring conclusive information specific on the shape and size of proteins remains challenge.

4. Conclusions

Time-resolved USAXS was successfully applied to pea and whey proteins gelation to track their changes of structural units in terms of size and shape. During the gelation process, both proteins underwent unfolding and formed loose structures which later aggregated to form surface fractals with dominant size of less than 30 nm. Those aggregates started to form at temperature below ~68 °C for both proteins. The average size of the aggregates changed slightly once being formed, but their amounts still increased, indicating protein aggregation occurred throughout the gelation process and not all proteins were involved in the aggregation at the same time. Compared to whey proteins, pea protein gels were composed of larger aggregates with higher polydispersity, which contributed to the more heterogenous and less continuous networks associated with lower gel strength.

Declaration of competing interest

The author declare they have no conflicts of interest.

Acknowledgements

We thank Dr. Daniel Veghte and Brian Kemmenoe for the help with the SEM.

Funding

This work was supported by the College of Food, Agricultural, and Environmental Science at the Ohio State University; This research used resources of the Advanced Photon Source, a U.S. Department of Energy (DOE) Office of Science User Facility, operated for the DOE Office of Science by Argonne National Laboratory under Contract No. DE-AC02-06CH11357. This research also used a facility supported by NIH/NINDS grands [P30 NS104177 and S10 OD026842].

Author contributions

DC: Conceptualization, data curation, formal analysis, investigation, methodology, writing-original draft

IK: investigation, methodology, data curation, writing- review & editing

JI: investigation, methodology, data analysis, writing- review & editing

LP: investigation, data analysis, writing- review & editing

OC: supervision, validation, methodology, funding acquisition, writing-review & editing

References

Ako, K., Durand, D., & Nicolai, T. (2011). Phase separation driven by aggregation can be reversed by elasticity in gelling mixtures of polysaccharides and proteins. *Soft Matter*, *7*, 2507-2516. DOI: 10.1039/C0SM01152E.

Aymard, P., Gimel, J. C., Nicolai, T., & Durand, D. (1996). Experimental evidence for a two-step process in the aggregation of *β*-lactoglobulin at pH 7. *Journal de Chimie Physique et de Physico-Chimie Biologique*, 93, 987-997. DOI : 10.1051/jcp/1996930987.

Banc, A., Pincemaille, J., Costanzo, S., Chauveau, E., Appavou, M. S., Morel, M. H., et al. (2019). Phase separation dynamics of gluten protein mixtures. *Soft Matter*, *15*, 6160-6170. DOI: 10.1039/C9SM00966C.

Banerjee, S., & Bhattacharya, S. (2012). Food gels: gelling process and new applications. *Critical Reviews in Food Science and Nutrition*, *52*, 334-346. https://doi.org/10.1080/10408398.2010.500234.

Beaucage, G. (1995). Approximations leading to a unified exponential/power-law approach to small-angle scattering. *Journal of Applied Crystallography*, *28*, 717-728. https://doi.org/10.1107/S0021889895005292.

Beaucage, G., Ulibarri, T. A., Black, E. P., & Schaefer, D. W. (1995). Multiple size scale structures in silica-siloxane composites studied by small-angle scattering. In *ACS symposium series* (pp. 97-111). American Chemical Society, Washington, DC.

Boye, J., Zare, F., & Pletch, A. (2010). Pulse proteins: Processing, characterization, functional properties and applications in food and feed. *Food Research International*, *43*, 414-431. https://doi.org/10.1016/j.foodres.2009.09.003.

Brodkorb, A., Croguennec, T., Bouhallab, S., & Kehoe, J. J. (2016). Heat-induced denaturation, aggregation and gelation of whey proteins. In P. L. McSweeney, & J. A. O'Mahony (Eds.), *Advanced dairy chemistry* (pp. 155-178). Springer, New York, NY.

Chen, D., Fang, F., Federici, E., Campanella, O., & Jones, O. G. (2020). Rheology, microstructure and phase behavior of potato starch-protein fibril mixed gel. *Carbohydrate Polymers*, *239*, 116247. https://doi.org/10.1016/j.carbpol.2020.116247.

Chen, D., Zhu, X., Ilavsky, J., Whitmer, T., Hatzakis, E., Jones, O. G., & Campanella, O. H. (2021). Polyphenols Weaken Pea Protein Gel by Formation of Large Aggregates with Diminished Noncovalent Interactions. *Biomacromolecules*, *22*, 1001-1014. https://doi.org/10.1021/acs.biomac.0c01753.

Chen, N., Zhao, M., Chassenieux, C., & Nicolai, T. (2017). The effect of adding NaCl on thermal aggregation and gelation of soy protein isolate. *Food Hydrocolloids*, *70*, 88-95. https://doi.org/10.1016/j.foodhyd.2017.03.024.

Comfort, S., & Howell, N. K. (2002). Gelation properties of soya and whey protein isolate mixtures. *Food Hydrocolloids*, *16*, 661-672. https://doi.org/10.1016/S0268-005X(02)00033-4.

Da Vela, S., Braun, M. K., Dörr, A., Greco, A., Möller, J., Fu, Z., et al. (2016). Kinetics of liquid–liquid phase separation in protein solutions exhibiting LCST phase behavior studied by time-resolved USAXS and VSANS. *Soft Matter*, *12*, 9334-9341. DOI: 10.1039/C6SM01837H.

Doster, W., & Longeville, S. (2007). Microscopic diffusion and hydrodynamic interactions of hemoglobin in red blood cells. *Biophysical Journal*, *93*(4), 1360-1368. https://doi.org/10.1529/biophysj.106.097956.

Fitzsimons, S. M., Mulvihill, D. M., & Morris, E. R. (2007). Denaturation and aggregation processes in thermal gelation of whey proteins resolved by differential scanning calorimetry. *Food Hydrocolloids*, *21*, 638-644.

Huang, X. L., Catignani, G. L., Foegeding, E. A., & Swaisgood, H. E. (1994). Comparison of the gelation properties of beta-lactoglobulin genetic variants A and B. *Journal of Agricultural and Food Chemistry*, *42*, 1064-1067. https://doi.org/10.1021/jf00041a003.

Ikeda, S., & Morris, V. J. (2002). Fine-stranded and particulate aggregates of heat-denatured whey proteins visualized by atomic force microscopy. *Biomacromolecules*, *3*, 382-389. https://doi.org/10.1021/bm0156429.

Ilavsky, J., & Jemian, P. R. (2009). Irena: tool suite for modeling and analysis of small-angle scattering. *Journal of Applied Crystallography*, *42*, 347-353. https://doi.org/10.1107/S0021889809002222.

Ilavsky, J., Jemian, P. R., Allen, A. J., Zhang, F., Levine, L. E., & Long, G. G. (2009). Ultra-small-angle X-ray scattering at the Advanced Photon Source. *Journal of Applied Crystallography*, *42*, 469-479. https://doi.org/10.1107/S0021889809008802.

Ilavsky, J., Zhang, F., Allen, A. J., Levine, L. E., Jemian, P. R., & Long, G. G. (2013). Ultra-small-angle X-ray scattering instrument at the advanced photon source: history, recent development, and current status. *Metallurgical and Materials Transactions A*, *44*, 68-76. https://doi.org/10.1007/s11661-012-1431-y.

Ilavsky, J., Zhang, F., Andrews, R. N., Kuzmenko, I., Jemian, P. R., Levine, L. E., et al. (2018). Development of combined microstructure and structure characterization facility for *in situ* and operando studies at the Advanced Photon Source. *Journal of Applied Crystallography*, *51*, 867-882. https://doi.org/10.1107/S160057671800643X.

Kaieda, S., Lund, M., Plivelic, T. S., & Halle, B. (2014). Weak self-interactions of globular proteins studied by small-angle X-ray scattering and structure-based modeling. *The Journal of Physical Chemistry B*, *118*, 10111-10119. https://doi.org/10.1016/j.foodhyd.2006.07.007.

Ko, S., & Gunasekaran, S. (2009). *In situ* microstructure evaluation during gelation of *β*-lactoglobulin. *Journal of Food Engineering*, *90*, 161-170. https://doi.org/10.1016/j.jfoodeng.2008.06.030.

Kornet, R., Penris, S., Venema, P., van der Goot, A. J., Meinders, M., & van der Linden, E. (2021). How pea fractions with different protein composition and purity can substitute WPI in heat-set gels. *Food Hydrocolloids*, 106891. https://doi.org/10.1016/j.foodhyd.2021.106891.

Kornet, R., Veenemans, J., Venema, P., van der Goot, A. J., Meinders, M., Sagis, L., & van der Linden, E. (2021). Less is more: Limited fractionation yields stronger gels for pea proteins. *Food Hydrocolloids*, *112*, 106285. https://doi.org/10.1016/j.foodhyd.2020.106285.

Mahmoudi, N., Mehalebi, S., Nicolai, T., Durand, D., & Riaublanc, A. (2007). Light-scattering study of the structure of aggregates and gels formed by heat-denatured whey protein isolate and β-lactoglobulin at neutral pH. *Journal of Agricultural and Food Chemistry*, *55*, 3104-3111. https://doi.org/10.1021/jf063029g.

McCann, T. H., Guyon, L., Fischer, P., & Day, L. (2018). Rheological properties and microstructure of soy-whey protein. *Food Hydrocolloids*, *82*, 434-441. https://doi.org/10.1016/j.foodhyd.2018.04.023.

McEwan, M. E., Egorov, S. A., Ilavsky, J., Green, D. L., & Yang, Y. (2011). Mechanical reinforcement of polymer nanocomposites: theory and ultra-small angle X-ray scattering (USAXS) studies. *Soft Matter*, *7*, 2725-2733. DOI: 10.1039/C0SM00393J.

Mehalebi, S., Nicolai, T., & Durand, D. (2008). The influence of electrostatic interaction on the structure and the shear modulus of heat-set globular protein gels. *Soft Matter*, *4*, 893-900. DOI: 10.1039/B718640A.

Miles, M. J., Morris, V. J., Carroll, V., Wright, D. J., & Newby, V. (1985). Small-angle X-ray scattering studies of 7S and 11S globulins from pea (*Pisum sativum*). *International Journal of Biological Macromolecules*, *7*, 125-126. https://doi.org/10.1016/0141-8130(85)90044-3.

Munialo, C. D., van der Linden, E., & de Jongh, H. H. (2014). The ability to store energy in pea protein gels is set by network dimensions smaller than 50 nm. *Food Research International*, *64*, 482-491. https://doi.org/10.1016/j.foodres.2014.07.038.

Nicolai, T. (2019). Gelation of food protein-protein mixtures. *Advances in Colloid and Interface Science*, *270*, 147-164. https://doi.org/10.1016/j.cis.2019.06.006.

Nicolai, T., Pouzot, M., Durand, D., Weijers, M., & Visschers, R. W. (2005). Iso-scattering points during heat-induced aggregation and gelation of globular proteins indicating micro-phase separation. *Europhysics Letters*, *73*, 299. 10.1209/epl/i2005-10391-8.

O'Kane, F. E., Happe, R. P., Vereijken, J. M., Gruppen, H., & van Boekel, M. A. (2004). Heat-induced gelation of pea legumin: Comparison with soybean glycinin. *Journal of Agricultural and Food Chemistry*, *52*, 5071-5078. https://doi.org/10.1021/jf035215h.

Picone, C. S., Takeuchi, K. P., & Cunha, R. L. (2011). Heat-induced whey protein gels: Effects of pH and the addition of sodium caseinate. *Food Biophysics*, *6*, 77-83. https://doi.org/10.1007/s11483-010-9177-9.

Porcar, L., Falus, P., Chen, W. R., Faraone, A., Fratini, E., Hong, K., et al. (2010). Formation of the dynamic clusters in concentrated lysozyme protein solutions. *The Journal of Physical Chemistry Letters*, *1*, 126-129. https://doi.org/10.1021/jz900127c.

Ramos, Ó. L., Pereira, J. O., Silva, S. I., Amorim, M. M., Fernandes, J. C., Lopes-da-Silva, J. A., et al. (2012). Effect of composition of commercial whey protein preparations upon gelation at various pH values. *Food Research International*, *48*, 681-689. https://doi.org/10.1016/j.foodres.2012.06.004.

Saluja, A., & Kalonia, D. S. (2008). Nature and consequences of protein–protein interactions in high protein concentration solutions. *International Journal of Pharmaceutics*, *358*(1-2), 1-15. https://doi.org/10.1016/j.ijpharm.2008.03.041.

Steyer, A. M., Schertel, A., Nardis, C., & Möbius, W. (2019). FIB-SEM of mouse nervous tissue: Fast and slow sample preparation. *Methods in Cell Biology*, *152*, 1-21. https://doi.org/10.1016/bs.mcb.2019.03.009.

Stone, A. K., Karalash, A., Tyler, R. T., Warkentin, T. D., & Nickerson, M. T. (2015). Functional attributes of pea protein isolates prepared using different extraction methods and cultivars. *Food Research International*, *76*, 31-38. https://doi.org/10.1016/j.foodres.2014.11.017.

Sun, X. D., & Arntfield, S. D. (2011). Gelation properties of salt-extracted pea protein isolate induced by heat treatment: Effect of heating and cooling rate. *Food Chemistry*, *124*, 1011-1016. https://doi.org/10.1016/j.foodchem.2010.07.063.

Sun, X. D., & Arntfield, S. D. (2012). Molecular forces involved in heat-induced pea protein gelation: effects of various reagents on the rheological properties of salt-extracted pea protein gels. *Food Hydrocolloids*, *28*, 325-332. https://doi.org/10.1016/j.foodhyd.2011.12.014.

Tsung, K. L., Ilavsky, J., & Padua, G. W. (2020). Formation and characterization of zein-based oleogels. *Journal of Agricultural and Food Chemistry*, *68*, 13276-13281. https://doi.org/10.1021/acs.jafc.0c00184.

Urbonaite, V., De Jongh, H. H. J., Van Der Linden, E., & Pouvreau, L. (2015). Water holding of soy protein gels is set by coarseness, modulated by calcium binding, rather than gel stiffness. *Food Hydrocolloids*, *46*, 103-111. https://doi.org/10.1016/j.foodhyd.2014.12.010.

Vijayalakshmi, L., Krishna, R., Sankaranarayanan, R., & Vijayan, M. (2008). An asymmetric dimer of β-lactoglobulin in a low humidity crystal form—Structural changes that accompany partial dehydration and protein action. *Proteins: Structure, Function, and Bioinformatics*, *71*, 241-249. https://doi.org/10.1002/prot.21695.

Vogtt, K., Javid, N., Alvarez, E., Sefcik, J., & Bellissent-Funel, M. C. (2011). Tracing nucleation pathways in protein aggregation by using small angle scattering methods. *Soft Matter*, *7*, 3906-3914. DOI: 10.1039/C0SM00978D.

Wagner, J., Biliaderis, C. G., & Moschakis, T. (2020). Whey proteins: musings on denaturation, aggregate formation and gelation. *Critical Reviews in Food Science and Nutrition*, *60*, 3793-3806. https://doi.org/10.1080/10408398.2019.1708263.

Weijers, M., Visschers, R. W., & Nicolai, T. (2002). Light scattering study of heat-induced aggregation and gelation of ovalbumin. *Macromolecules*, *35*, 4753-4762. https://doi.org/10.1021/ma0120198.

Woldeyes, M. A., Qi, W., Razinkov, V. I., Furst, E. M., & Roberts, C. J. (2020). Temperature dependence of protein solution viscosity and protein–protein interactions: insights into the origins of high-viscosity protein solutions. *Molecular Pharmaceutics*, *17*, 4473-4482. https://doi.org/10.1021/acs.molpharmaceut.0c00552.

Xiao, J., Shi, C., Zhang, L., Li, Y., Qi, J., Wang, Y., & Huang, Q. (2016). Multilevel structural responses of *β*-conglycinin and glycinin under acidic or alkaline heat treatment. *Food Research International*, *89*, 540-548. https://doi.org/10.1016/j.foodres.2016.09.006.

Yang, J., Zamani, S., Liang, L., & Chen, L. (2021). Extraction methods significantly impact pea protein composition, structure and gelling properties. *Food Hydrocolloids*, *117*, 106678. https://doi.org/10.1016/j.foodhyd.2021.106678.

667